IEEE Access
Multidisciplinary | Rapid Review | Open Access Journal

Received January 24, 2021, accepted February 18, 2021, date of publication February 22, 2021, date of current version March 1, 2021.

Digital Object Identifier 10.1109/ACCESS.2021.3060947

Underwater Image Restoration and Enhancement Based on a Fusion Algorithm With Color Balance, Contrast Optimization, and Histogram Stretching

WEILIN LUO, (Member, IEEE), SHUNQIANG DUAN, AND JIWEN ZHENG
College of Mechanical Engineering and Automation, Fuzhou University, Fuzhou 350108, China
Corresponding author: Weilin Luo (wlluo@fzu.edu.cn)

This work was supported in part by the Fujian Provincial Department of Ocean and Fisheries, China, under Grant MHGX-16.

ABSTRACT A fusion algorithm is proposed for the restoration and enhancement of underwater images. Color balance, contrast optimization and histogram stretching are carried out. To alleviate the effect of color shift in an underwater image, the scalar values of R, G, B channels are renewed so that the distributions of the three channels in histogram are similar. Instead of refining the transmittance in dark channel prior based restoration, an optimized contrast algorithm is employed by which the optimal transmittance is determined. To further improve the brightness and contrast of underwater images, a histogram stretching algorithm based on the red channel is given. To verify the effectiveness of the proposed fusion algorithm, experimental underwater images are treated. Results show that the quality of underwater images is improved significantly, both in term of subjective visual effect and objective evaluation. The proposed underwater image processing strategy is also compared with some popular techniques. Comparison results indicate the advantage of the proposed strategy over others.

INDEX TERMS Underwater image, restoration, enhancement, color balance, contrast, histogram, dark channel prior.

I. INTRODUCTION

In the human exploration and exploitation of ocean, the underwater mission is challenging. The acquisition and analysis of underwater information is vital to accomplish underwater missions like underwater object localization [1], marine life recognition [2], underwater archeology [3], underwater environment monitoring [4], underwater search and salvage [5], underwater maintenance [6], etc. Underwater optical image provides an important source of underwater information. However, due to the characteristic attenuation and scattering of light in water, underwater images through camera sensors are apt to degrade. Typically, the attenuation results in color shift while scattering of light makes an underwater image blurred and a decrease of contrast. Although the physical characteristics of underwater light emission have a great impact on underwater images, they are not the only phenomena that affect underwater visibility and quality of underwater images. For example, the movement of water or fish shoal can cause so-called motion blur [7]. Dissolved organisms and tiny suspended particles in waters often lead to noises in underwater images and the influence of light backscattering on underwater imaging will be amplified. Representative noises include salt-and-pepper noise, Gaussian noise and marine snow. It is noted that marine snow is a very specific but ubiquitous noise for underwater conditions, caused by biological and mineral particles, or bubbles [8]. Marine snow results in additional light backscattering which manifests in images as white blobs of various size and shape, which negatively affects underwater visibility [9], [10].

To obtain high-quality underwater images, one can resort to an advanced imaging equipment like the divergent-beam underwater Lidar imaging (UWLI) system [11] or multistate underwater laser line scan system [12]. The main obstacle for users is the expensive cost with the equipment. Another alternative to obtain high-quality underwater images is the technique of image processing. It is characterized by high efficiency and low cost. In recent years, underwater image processing has become a hot topic in underwater technology.

Generally, underwater image processing concerns two techniques, i.e. image restoration and enhancement. Image restoration is based on a physical model about original image

The associate editor coordinating the review of this manuscript and approving it for publication was Quansheng Guan.

and recovered image. Degradation of image is focused in a restoration process. For image enhancement, the focus is mainly on the enhancement of pixels of images according to some subjective qualitative criteria, rather than the degradation process and the physical model of imaging for image restoration. From the point of view of calculation burden, image enhancement approaches are usually simpler and faster than image restoration approaches in which convolution and deconvolution operation are conducted [13]. During the last decade, many kinds of underwater image enhancement algorithms have been proposed. Commonly used methods include histogram equalization, wavelet transform and Retinex algorithm. Over the past decade, these classic algorithms have been applied widely and developed. For example, Iqbal *et al.* [14] proposed an enhancement method based on histogram sliding stretching. Henke *et al.* [15] proposed a color constancy hypothesis algorithm based on gray world hypothesis to solve the color distortion problem of underwater images. Guraksin *et al.* [16] addressed the use of a method formed by the wavelet transform and the differential evolution algorithm. Tang *et al.* [17] presented the underwater image and video enhancement based on Retinex. Although these enhancement algorithms can process underwater images and have been widely used, there exist some inherent shortcomings. For histogram equalization, image enhancement is carried out by obtaining a histogram with approximately uniform distribution. However, some details of the processed image might disappear. Moreover, there might be excessive enhancement at the peak of histogram. For wavelet transform, it is usually successful to deal with images captured in shallow waters, while fails in deep waters where the red light attenuation is severe. For Retinex algorithm, adaptive enhancement can be achieved by pixel dynamic range compression, edge enhancement and color constancy. However, halo effect might produce in areas with large brightness difference. In recent years, some improvement of classic underwater image enhancement methods should be noted for example the Rayleigh stretching proposed by Abdul Ghani and Isa [18]–[22]. Moreover, a popular machine learning method, deep learning, has been applied to the enhancement of underwater images, for examples [23]–[28]. Convolutional neural networks (CNN) and generative adversarial networks (GAN) are the representative approaches. However, due to the lack of ground truth in underwater environments, the feasibility of this kind of supervised machine learning approach needs to be further confirmed.

Due to the inherit disadvantage of each algorithm in enhancing underwater images, fusion algorithms are preferred for more and more researchers. For example, Ghani [29] proposed an integration of recursive-overlapped contrast limited adaptive histogram specification and dual-image wavelet fusion to enhance underwater image contrast. Ancuit *et al.* [30] proposed a fusion algorithm in which the techniques of wavelet transform, histogram stretching and color correction are combined. Qiao *et al.* [31] proposed an algorithm based on histogram equalization and wavelet transform to achieve underwater image quality enhancement.

Due to the particularity of underwater environment, the restoration of underwater images becomes more challenging than an image captured in air. Generally, linear physical model and optical physical propagation model are available to obtain a restoration underwater image. Comparatively, the optical physical propagation model gains more attention. Trucco and Olmos-Antillon [32] put forward an adaptively adjusted restoration filter based on the simplified Jaffe-McGlamery light propagation model proposed by Jaffe [33]. Wang *et al.* [34] used the quadratic function fitting to eliminate the effect of posterior scattering based on an underwater light propagation model. Wanger *et al.* [35] proposed a visual quality perception method based on light propagation model. Shi *et al.* [36] proposed a normalised gamma transformation-based contrast-limited adaptive histogram equalisation with colour correction.

Because of the similarity between underwater environment and foggy outdoors, dehazing algorithms are in common use to obtain restoration underwater images. A representative algorithm is the dark channel prior algorithm (DCP) raised by He *et al.* [37]. Carlevaris-Bianco *et al.* [38] used the difference in attenuation of the RGB channels of the underwater image to estimate the depth of the scene. Galdran *et al.* [39] presented a red channel algorithm to recover colors associated with short waves. Wang *et al.* [40] designed a patch-based dark channel prior dehazing for RS multi-spectral image. Kansal and Kasana [41] proposed minimum preserving subsampling-based fast image de-fogging. Yu *et al.* [42] proposed an underwater image dehazing algorithm based on DCP and depth transmission map. The main difficulty with DCP is the limitation in processing images of white object or the images with white background.

In the study, the restoration and enhancement of underwater images are investigated. To obtain high-quality underwater images, a fusion algorithm is proposed that refers to color balance, contrast enhancement and histogram stretching. In the study, the contribution to color balance is the reallocation of the single channel value of the three color channels. The contribution to histogram stretching is that the algorithm is based on the average single channel value of red channel. Instead of refining the transmittance in DCP based restoration conventionally, an optimized contrast algorithm is employed by which the optimal transmittance can be determined. To demonstrate the validity of the proposed fusion algorithm, some underwater images with obvious color deviation and different ambiguity are processed and compared with several commonly used algorithms. In the study, some of the underwater images to be processed are taken from datasets RUIE [43], some from internet and the others from experiments. Comparison results show that the proposed algorithm can effectively improve the quality of underwater images, including the removal of color distortion, and improvement of contrast and clarity as well.

II. FUNDAMENTALS OF UNDERWATER IMAGING

The propagation of light differs in water and air. In the light propagation in water, there are several important factors that result in attenuation and scattering of light. The density of water is greater than air, which causes the attenuation of light. Water selectively scatters and absorbs certain wavelengths of visible light. Suspended particles in water affect the light transmission and produce scattering of light. Various types of noise occur for example marine snow that causes additional light backscattering. Temperature and salinity also cause the light scattering [44]. To summarize, the light attenuation and scattering are more serious in water than air. As a result, underwater optical images are apt to blur along with lower contrast.

The light received by an underwater camera can be divided into three components: direct component, forward scattered component and backward scattered component. The total light intensity received by the camera sensor can be expressed as [33]:

$$E_T = E_d + E_f + E_b, \tag{1}$$

where E_T represents the total light intensity; E_d the direct component; E_f the forward scattered component; E_b the backward scattered component. The three components can be calculated as follows. For direct component, it can be calculated as:

$$E_d = Je^{-cd}, \tag{2}$$

where J is the reflection part from the object after receiving light from an illumination source; c is the attenuation coefficient; d is the distance between the object and the sensor. For forward scattered component, it is given by:

$$E_f = E_d * g = Jt * g, \tag{3}$$

where g is the point spread function (PSF) for predicting beam propagation and imaging system performance [45], [46]. t is defined as $t = e^{-cd}$. As can be seen from Eq.(3), the forward scattered component E_f is the convolution of the direct component and PSF. For backward scattered component, it can be expressed as:

$$E_b = B_\infty(1 - t), \tag{4}$$

where B_∞ represents the background light at infinity in the image.

Based on Eqs.(2)-(4), the total light energy can be determined. Because the effect of forward scattered component E_f on underwater imaging is much smaller than that of direct component and backward scattered component, the forward scattered component can be ignored in the calculation of total light intensity. As a result, the simplified underwater imaging model can be expressed as:

$$E_T = Jt + B_\infty(1 - t). \tag{5}$$

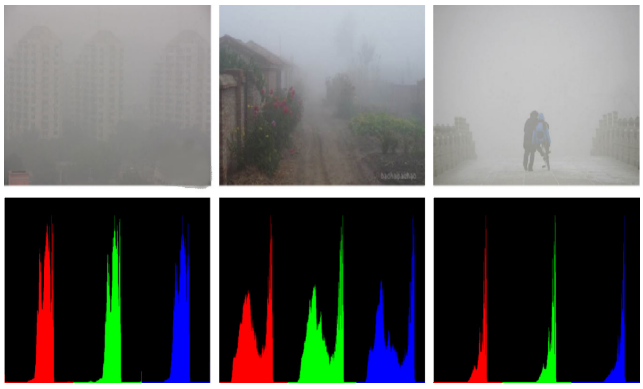

FIGURE 1. Foggy images and histograms.

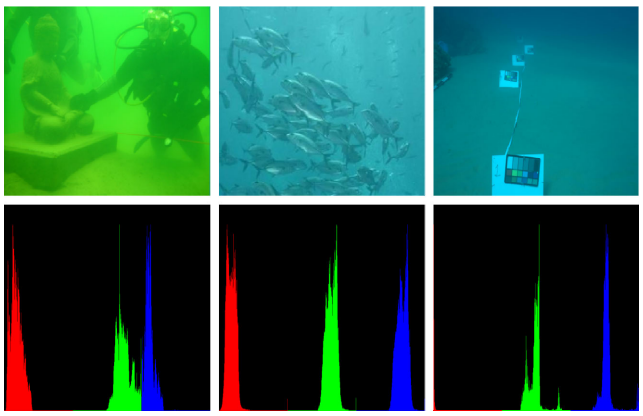

FIGURE 2. Underwater images and histograms.

III. METHOD DESCRIPTION

To improve the quality of underwater images, three strategies are proposed including a color balance algorithm, an optimized contrast algorithm and a histogram stretching algorithm based on red channel.

A. COLOR BALANCE ALGORITHM

Seemingly, an image obtained in foggy environment and an image obtained in underwater environment are similar. Therefore, some dehazing algorithms (e.g. DCP) are applied to deal with underwater images. However, the results are not satisfactory. The main reason is that the attenuation of light differs in different environments. In outdoor foggy environments, the attenuations of lights with different wavelengths are almost the same. While in underwater environments, the attenuations of lights vary with wavelengths. Fig. 1 displays three randomly selected foggy images and their corresponding histograms. It can be seen that the histograms of different channels (three channels for a RGB image) are very similar, including the peaks, troughs, and grayscales. As a contrast, Fig.2 presents three randomly selected underwater images and corresponding histograms. As can be seen, the color deviation of the underwater images is severe and the contrast is seriously degraded. The peaks and troughs of the different channels of the first two underwater images are similar, except that the single channel values

corresponding to the peaks and troughs are different. It is noted that the third picture is taken in the deep sea without light illumination. In this case, the red light with a longer wavelength is absorbed. Correspondingly, the component of red channel in the histogram vanishes. Differently, the components of blue and green channel are kept and are similar in terms of distribution.

To alleviate the effect of color shift, a color balance algorithm is proposed by which the single channel value of the histogram in each color channel of an underwater image is moved to a similar position. Using this method, firstly the average single channel values of three channel components of R, G, and B are calculated respectively, expressed by m_R, m_G and m_B.

Secondly, the average scalar value of the average single channel values of R, G and B channels can be obtained as:

$$m_{ave} = (m_R + m_G + m_B)/3. \tag{6}$$

The differences between the average single channel value m_R, m_G, m_B and the mean scalar value m_{ave} can be determined as:

$$\begin{cases} d_R = m_{ave} - m_R \\ d_G = m_{ave} - m_G \\ d_B = m_{ave} - m_B, \end{cases} \tag{7}$$

Eventually the single channel value of the three channels of R, G, and B can be moved to similar positions by:

$$\begin{cases} R' = R + d_R \\ G' = G + d_G \\ B' = B + d_B, \end{cases} \tag{8}$$

where R', G', and B' are the pixel values of the R, G, and B channel components of the processed image. As can be recognized, the single channel values of the three channels are modified to the same level, which can effectively eliminate the effect of color shift. It should be noted that the proposed algorithm to reorganize the single channel value of three channels is partially the same as the gray world algorithm. However, white balance based on the proposed algorithm can provide a more satisfactory result than the gray world algorithm, especially when the light intensity of red channel is negligible. Table 1 presents the pseudo-code of the color balance algorithm.

To prove the effectiveness of the proposed color balance algorithm, it is compared with gray world algorithm, one of the most commonly used algorithms in image enhancement. Fig. 3 presents the comparison results. As can be seen, overall tone of the images after processing is reddish by means of gray world algorithm. Even overexposure happens to some image like No.4 image. On the contrary, the proposed color balance algorithm does not produce obvious color deviation, neither overexposure.

TABLE 1. Pseudo-code of color balance algorithm.

Algorithm1 Color Balance Algorithm
Input: degraded underwater images
Output: underwater images after color balance
1: Calculate the average single channel value of each channel of R, G and B respectively. Then find the average scalar value by (6).
2: Compare m_{ave} and the average single channel values of m_R, m_G and m_B, determine the difference of single channel value d_R, d_G and d_B by (7).
3: According to the results of step2 and the single channel values of three channels, move the single channel values of three channels to a similar position by (8).
4: **Return** processed images

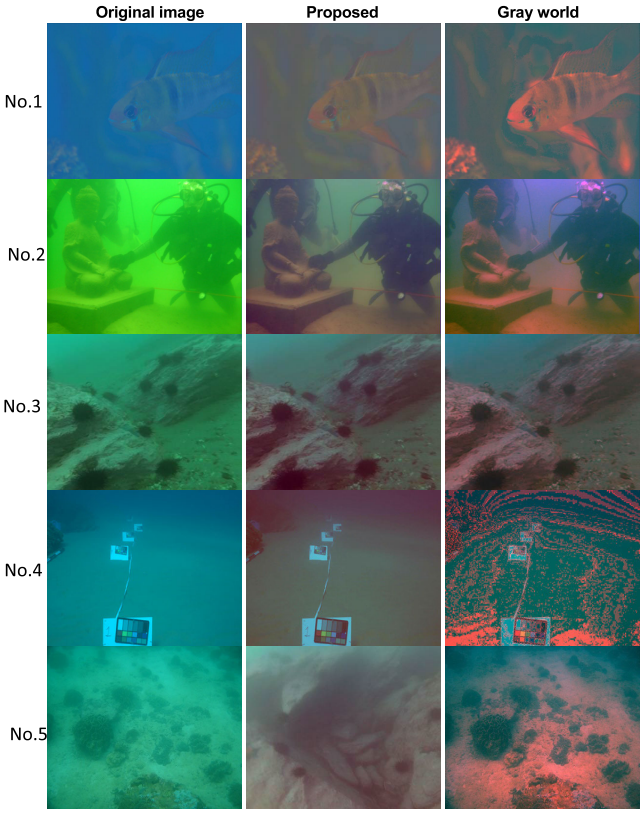

FIGURE 3. Comparison between gray world algorithm and proposed color balance algorithm.

B. OPTIMIZED CONTRAST ALGORITHM

Although the proposed color balance algorithm can alleviate the color shift in an underwater image, the contrast of the image needs to be improved. In the paper, an optimized contrast algorithm is employed. It is an extension of the dark channel prior dehazing algorithm. Instead of refining the transmittance, the optimized contrast algorithm provides a new way to determine the transmittance [47].

The restoration model can be described as:

$$I(x) = J(x)t(x) + A(1 - t(x)), \tag{9}$$

where $I(x) = \left[I_r(x), I_g(x), I_b(x)\right]^{\mathrm{T}}$ represents the RGB image received by the camera sensor; $J(x) = \left[J_r(x), J_g(x), J_b(x)\right]^{\mathrm{T}}$ represents the image after restoration; $A = \left[A_r, A_g, A_b\right]^{\mathrm{T}}$ represents the background light of the surrounding environment;

$t(x) \in [0, 1]$ is the transmittance of the image, which is determined by the distance between the scene point and the camera sensor. Usually, $t(x)$ is inversely proportional to the depth of the scene. As can be seen from (9), the estimation of A and $t(x)$ exerts an important influence on the restoration of the image.

To estimate the background light A, a method derived from the dehazing algorithm [4] is used. The quadtree space division is introduced to search area of the background light in a layer-by-layer way. By this method, the image is first divided into four areas. Then the variances of pixels in four areas can be calculated and the smallest variance can be determined. Division operation is repeated in the area with the smallest variance. Until the size of the selected area is less than a predefined threshold, division stops. In the study, the threshold is set as $n*0.001$, where n is the total number of pixels in the image.

Eq.(9) can be rewritten as:

$$J(x) = \frac{1}{t(x)}(I(x) - A) + A. \tag{10}$$

As can be recognized, the quality of the image after restoration depends on the transmittance $t(x)$ if the background light A is determined. An index is defined to evaluate the contrast of an image:

$$C_i = \sum_{x=1}^{N} \frac{(J_i(x) - \overline{J_i})^2}{N}, \tag{11}$$

where $i \in \{r, \ g, \ b\}$ represent the color channel; $\overline{J_i}$ is the average of the $J_i(x)$; N is the number of pixels in the divided area. Combined with (10), (11) becomes as:

$$C_i = \sum_{x=1}^{N} \frac{(I_i(x) - \overline{I_i})^2}{t^2 N}, \tag{12}$$

A complex contrast performance can be defined as:

$$E_c = -\sum_{i\in\{r,g,b\}} \sum_{x=1}^{N} \frac{(I_i(x) - \overline{I_i})^2}{t^2 N}. \tag{13}$$

Obviously, the contrast performance E_c can be viewed as a function of the transmittance t, i.e. $E_c = f(t)$. Furthermore, the minimization of E_c can be achieved by the optimization of t. From the definition of E_c, it can be inferred that an decrease of E_c denotes an increase of the contrast of an image.

Although the contrast can be improved by minimization of E_c, some pixel values might exceed the range of (0, 255). Therefore, an information loss function is taken as:

$$E_l = \sum_{i\in\{r,g,b\}} \sum_{x=1}^{N} \{(\min\{0, J_i(x)\})^2 + (\max\{0, J_i(x) - 255\})\}, \tag{14}$$

Furthermore, a comprehensive contrast performance index can be obtained as:

$$E = E_c + \lambda_L E_l, \tag{15}$$

TABLE 2. Pseudo-code of optimized contrast algorithm.

Algorithm2 Optimized Contrast Algorithm
Input: underwater images after color balance
Output: underwater images after optimized contrast
1: Estimate the background light A by the space partition method of quadtree.
2: According to the image contrast measurement formula (11), calculate the contrast value C_i by (12) and complex contrast performance index E_c by (13).
3: To prevent the pixel value exceeding the allowable range, define information loss function E_l as (14).
4: Obtain total cost function $E = E_c + \lambda_L E_l$ by (15) according to the imaging model, determine the best transmittance t as (16) by minimizing E
5: Through the background light A and the best transmittance t, obtain the image with optimized contrast, on the basis of underwater imaging models (9) and (10).
6: **Return** processed images

where λ_L is a factor reflecting the tradeoff between E_c and E_l. In the study, λ_L is selected as 5 by reference to [48]. An optimized transmittance t^* is determined by:

$$t^* = \arg\min E. \tag{16}$$

Table 2 presents the pseudo-code of the optimized contrast algorithm.

C. HISTOGRAM STRETCHING ALGORITHM BASED ON RED CHANNEL

To further improve the brightness and contrast of an underwater image, histogram stretching is conducted. It is known that the water environment has selective absorption of different colors of light. Red light is the most severely attenuated, especially in deep water. The problem of excessive compensation of the red channel occurs for most image enhancement algorithms. In the study, a histogram stretching algorithm based on the red channel is proposed. In the algorithm, the operation of histogram stretching depends on the intensity of red light. A scalar value threshold denoted by R is set to evaluate the attenuation of red light. An average single channel value R_{ave} of the red channel is firstly calculated as

$$R_{ave} = \frac{1}{n}\sum_{1}^{n} R_i, \tag{17}$$

where R_i is the single channel value of every pixel, n is the total number of pixels.

Then R_{ave} is compared with the threshold R to evaluate the red light attenuation. If the average single channel value of the red channel, denoted by R_{ave}, is greater than or equal to R, i.e., $R_{ave} \geq R$, the attenuation of red light is regarded as slight; whereas if $R_{\text{ave}} < R$, the attenuation of red light is regarded as heavy. In the case of slight attenuation of red light, histogram stretching is conducted with respect to three channels, i.e. R, G and B channels. While in the case of heavy attenuation of

TABLE 3. Pseudo-code of histogram stretching algorithm based on red channel.

Algorithm3 Histogram Stretching Algorithm Based on Red Channel
Input: underwater images after optimized contrast
Output: underwater images after histogram stretching
1: Calculate the average single channel value R_{ave} of red channel using (17). Set a scalar value threshold R, compare R_{ave} and R.
2: Set h_t as n*0.225%.
3: If $R_{ave} \geq R$, the attenuation of red light is regarded as slight, histogram stretching is conducted with respect to three channels, by using (18)
4: If $R_{ave} <$ R, the attenuation of red light is regarded as heavy, histogram stretching is only conducted with the G and B channels, by using (18)
5: **Return** the histogram stretched images.

red light, histogram stretching is only conducted with the G and B channels. The R channel remains unchanged to prevent excessive compensation.

The histogram stretching adopts the algorithm as:

$$I^c_{new}(i,j) = \begin{cases} 0 & I^c_{\text{old}}(i,j) < i^c_{\min} \\ 255 \times \dfrac{I^c_{old}(i,j) - i^c_{\min}}{i^c_{\max} - i^c_{\min}} & i^c_{\min} \leq I^c_{\text{old}}(i,j) \leq i^c_{\max} \\ 255 & I^c_{\text{old}}(i,j) > i^c_{\max}, \end{cases} \tag{18}$$

where c is with R, G, B channels if $R_{ave} \geq R$, while G, B channels if $R_{\text{ave}} < R$; i_{min} the minimal scalar value; i_{max} the maximal scalar value; $I^c_{new}(i,j)$ represents the updated scalar value at pixel point (i,j) after the histogram is stretched; $I^c_{old}(i,j)$ is the original scalar value at the same point. Both the minimal scalar value i_{min} and maximal scalar value i_{max} are determined by a threshold of pixel number h_t. In the study, a satisfactory threshold h_t is selected as n*0.225% by trials.

Table 3 presents the pseudo-code of the histogram stretching algorithm based on red channel.

IV. RESULTS AND ANALYSIS

The above three algorithms are proposed to deal with underwater images. The process can be depicted as Fig.4. Firstly, the color balance algorithm is applied to eliminate the color distortion. Optimized contrast algorithm is then used to improve the contrast of the image and decrease the backscatter effect. Histogram stretching based on red channel is finally conducted to improve the contrast and brightness of the underwater image.

A. VISUAL EFFECT

A set of ablation experiments are conducted to verify the effectiveness of each module (i.e. algorithm). As required, each module is gradually removed. Results are presented in Fig. 5. The images in left column (labeled with A3) are processed by proposed fusion algorithm in which color

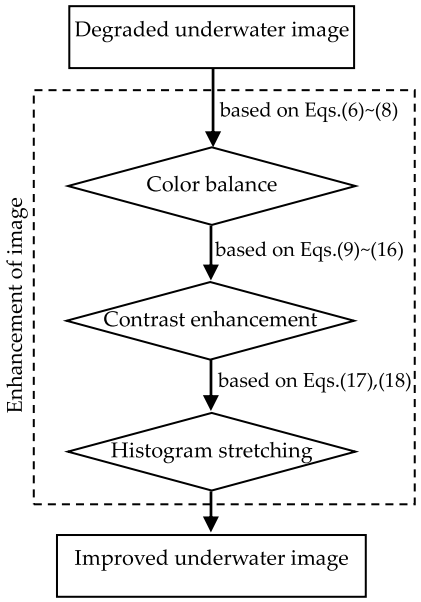

FIGURE 4. Process of enhancement of underwater images.

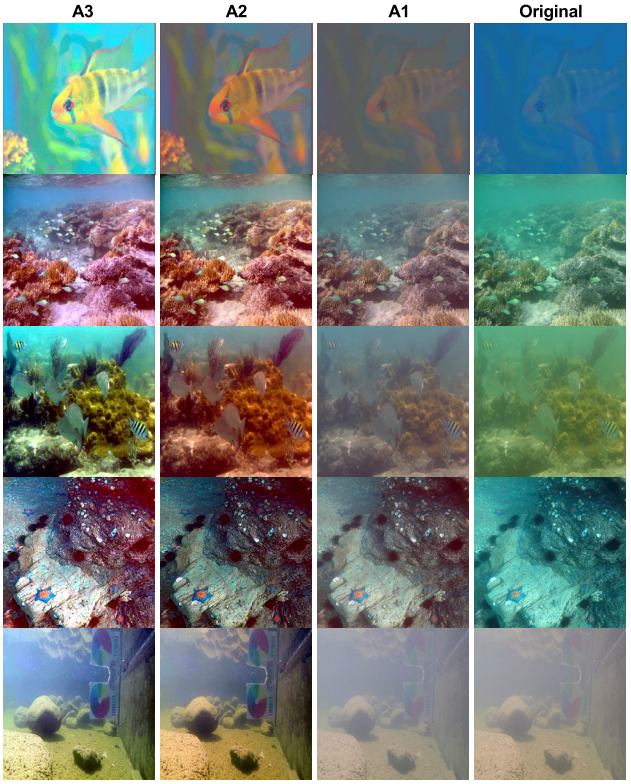

FIGURE 5. Ablation experiments.

balance, optimized contrast and histogram stretching based on red channel are combined. By ablation operation, for the images in the second column labeled with A2, color balance and optimized contrast remain. For the images in the third column labeled with A1, color balance is only kept.

As can be seen, good processing results can be achieved by using proposed fusion algorithm. Moreover, each module

or algorithm contributes to the final image quality. It is noted that for the images in the final row, there is no difference between the original image and A1 which is processed by proposed color balance algorithm. The reason is that the original picture is taken at two-meter water depth, which means no obvious color deviation occurs. In that case, the proposed color balance algorithm even does not produce an extra effect, which verifies the effectiveness of the proposed algorithm.

To further verify the effectiveness of the proposed fusion strategy, it is used to process several kinds of underwater images including those from dataset RUIE, some frequently used underwater images on internet and some underwater images from experiments. Comparison is conducted with popularly used algorithms, including Multi-scale Retina Enhancement Algorithm with Color Restoration (MSRCR), Red Channel Prior Algorithm (RCP), Underwater Dark Channel Prior Algorithm (UDCP), and modern algorithms including Generative Adversarial Networks (GAN) [49] and Recursive Adaptive Histogram Image Modification (RAHIM) [22]. Eighteen underwater images are selected and labelled with No.1∼18. Color shift happens to images No.1∼6. Specifically, the overall tone of images No. 1∼3 is bluish, while the overall tone of images No. 4∼6 is greenish. Definition degrades in images N0.7∼10. Images No.11∼13 are from UCCS sub-dataset in the RUIE dataset, while images No.14∼16 are from UIQS sub-dataset in the RUIE dataset. Images No.17∼18 are obtained in underwater experiments, characterized by back light and forward light respectively. Thus, five groups of image can be formed by viewing images No.11∼16 as a group. The comparison results are given in Fig.6. The first column is the original images; the following columns are respectively with MSRCR, RCP, UDCP, GAN, RAHIM and the proposed method in the study.

As can be recognized from the comparison, the proposed image enhancement strategy produces better results, in terms of definition, contrast, color balance, texture details and edge characteristics. The visual effect is more satisfactory. For MSRCR algorithm, the color distortion of blue-green channels can be effectively alleviated. However, excessive compensation of red channel happens to images No.2 and No.3. Moreover, the processed image is too bright, and the overall appearance is grayish. The definition is not improved obviously. For RCP algorithm, the color balance and contrast of images can be improved. However, it is not a good choice for processing greenish images, as shown in images No.4 and No.5 that, images are still greenish. Moreover, the definition needs to be improved by using RCP. For UDCP algorithm, the contrast and definition of images can be improved. The texture details are also enhanced. However, the color balance effect is not satisfactory. For GAN algorithm, the effects of defogging and contrast enhancement are not obvious. In contrast, GAN treatment is more effective in color balance.

RAHIM algorithm provides an effective way to enhance underwater images. In general, the underwater images can be well processed. Especially some images can be treated excellently for example the images No.6, No.7, No.10, No.11 and No.13. However, it is noted that the stability of the approach needs to be improved to avoid some unpredictable phenomena such as distortion (image No.2), over-enhancement (images No.1, and No.18), and additional noise (images No.4, No.5 and No.8).

To further illustrate the effectiveness and feasibility of the proposed strategy in underwater images, edge detection is performed. Edge information is one of important features of an image. For an image with higher contrast and definition, its edge is more obvious. In the study, the commonly used canny edge detection [50] is employed. Five representative images are drawn from the above five groups of images. In detail, image No.1 is taken from the first group, No.5 from second group, No.8 from the third group, No.16 from the fourth group and No.17 from the fifth group. Fig.7 shows the comparison results. As can be seen, the edge information obtained by using the proposed strategy in the study is much richer than by MSRCR, RCP, UDCP and GAN algorithms. For RAHIM algorithm, results show that it produces excessive edge information. In contrast, the proposed algorithm gains more accurate edge information, which verifies the effectiveness and feasibility of the proposed combination algorithm in the study.

B. OBJECTIVE EVALUTION

Since the evaluation of visual effect is influenced by human subjective consciousness, objective evaluation is necessary to verify the enhancement measures adopted in image processing. In the study, some classic objective evaluation indicators are used, i.e. contrast, UCIQE (underwater color image quality evaluation), PSNR (peak signal-to-noise ratio) and SSIM (structural similarity).

Generally speaking, the higher the contrast is, the better quality an image has. RMS (root mean square) contrast [51], Weber contrast [52], and Michelson contrast [53] are commonly used indices. In the study, the RMS contrast is employed, with the form as:

$$\sigma_{I_{w\times h}} = \sqrt{\frac{1}{w\times h}\sum\left(I(x,y) - \frac{1}{w\times h}\sum I(x,y)\right)^2}, \quad (19)$$

where $\sigma_{I_{w\times h}}$ represents the RMS contrast of an image with the dimension of $w \times h$; $I(x, y)$ is the pixel value at the point (x, y).

UCIQE is a comprehensive evaluation index that can reflect the overall quality of an image, referring to chroma, luminance contrast and saturation. Generally, a higher UCIQE value represents the better quality of an image. UCIQE index can be described as [54]:

$$UCIQE = c_1 \times \sigma_c + c_2 \times C_l + c_3 \times \mu_s, \quad (20)$$

where σ_c represents the deviation of chroma; C_l is the luminance contrast; μ_s is the average saturation; $c_i (i = 1, 2, 3)$ the weighted coefficients. In the study, the coefficients are

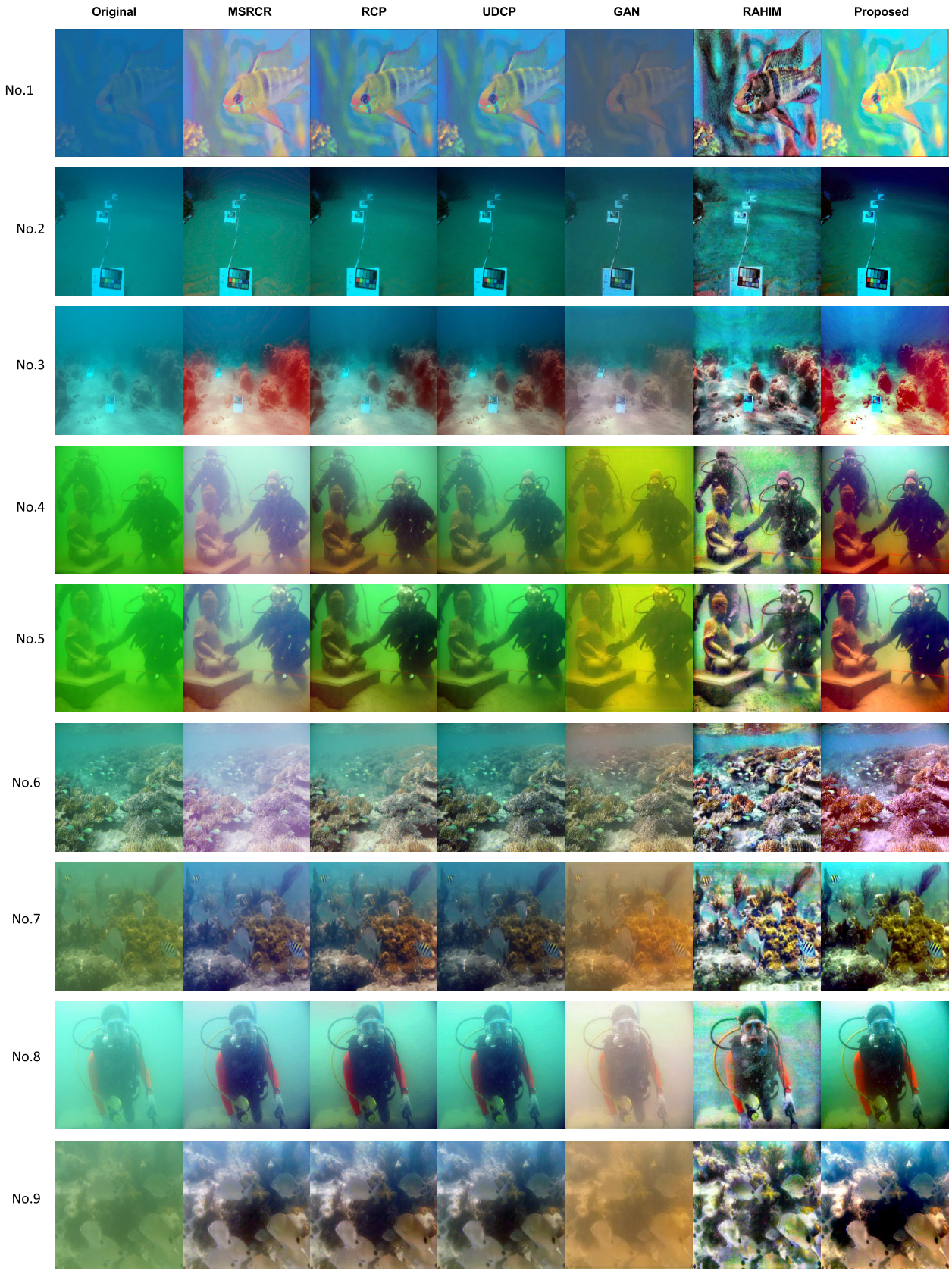

FIGURE 6. Enhancement of underwater images and comparison.

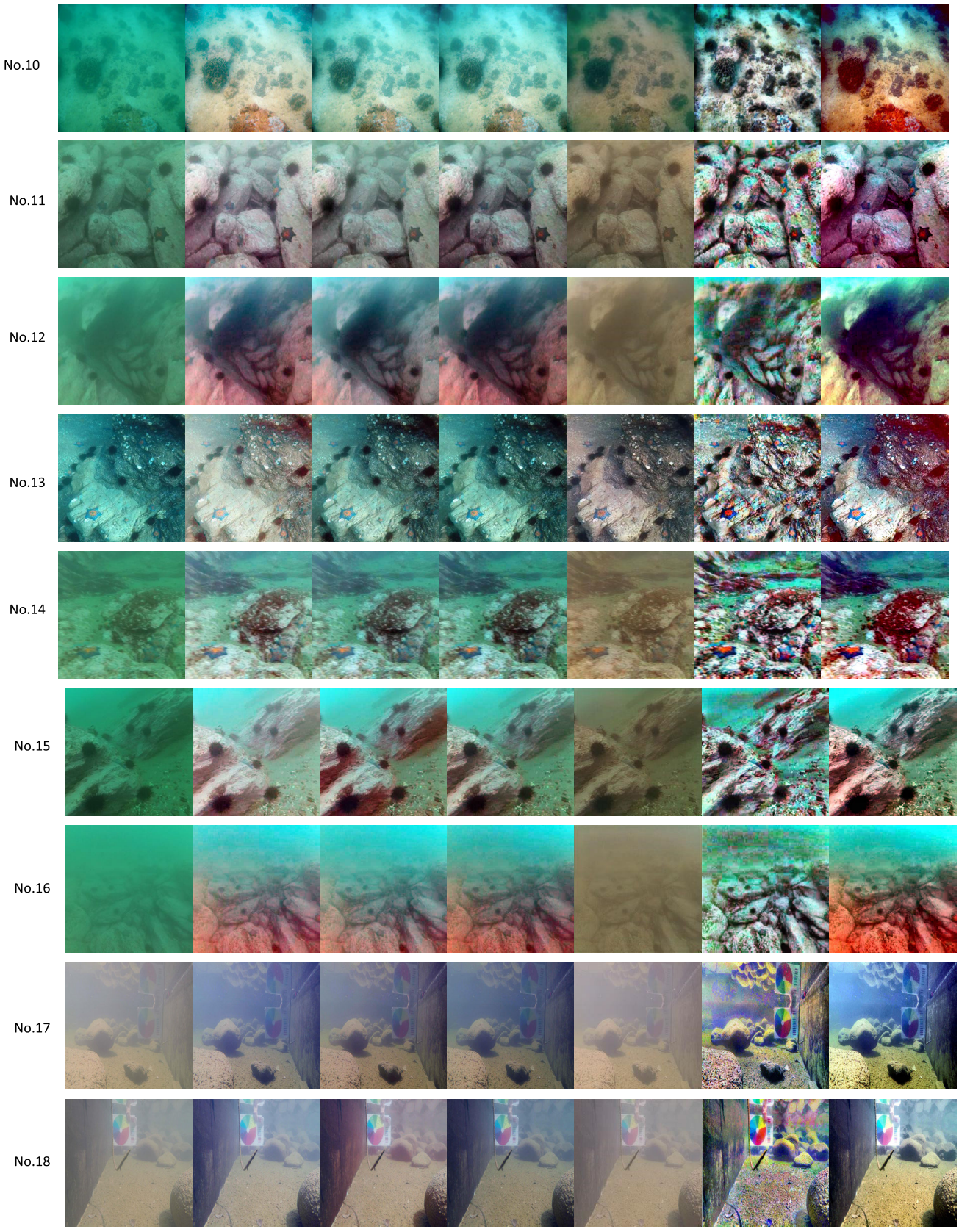

FIGURE 6. *(Continued.)* **Enhancement of underwater images and comparison.**

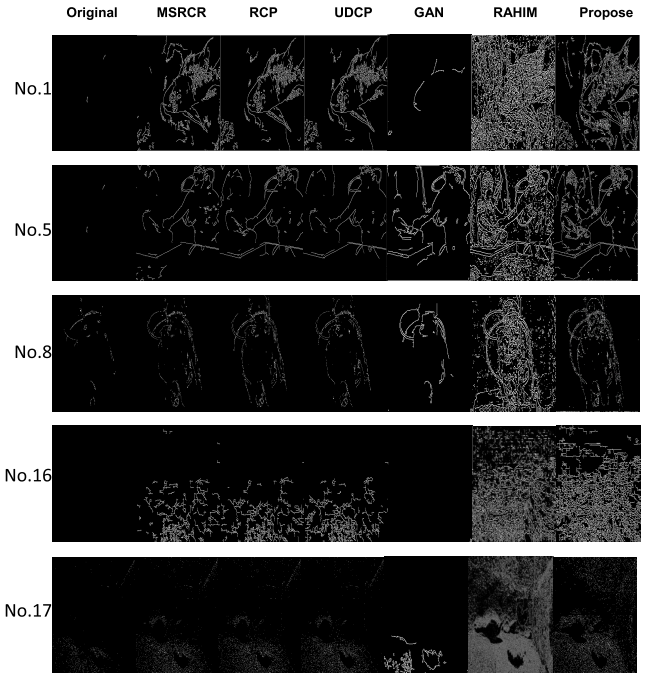

FIGURE 7. Edge detection.

selected as:

$$c_1 = 0.4680,\ c_2 = 0.2745,\ c_3 = 0.2576.$$

PSNR is a widely used objective metric for image evaluation. It is based on pixel error. A corresponding error sensitivity can be defined to measure whether the processing results are satisfactory. The larger the PSNR value is, the less distortion happens. PSNR can be described as [55]:

$$MSE = \frac{1}{w \times h} \sum_{i=0}^{w-1} \sum_{j=0}^{h-1} [I(i,j) - K(i,j)]^2 \tag{21}$$

$$PSNR = 10 \times \log_{10} \left(\frac{(2^n - 1)^2}{MSE} \right) \tag{22}$$

where I represents a processed image with the dimension $w \times h$ while K is the original image with the same dimension. MSE is the loss function. n is the number of bits for pixel, usually taken as 8 for underwater images.

SSIM is an index to measure the similarity of two digital images, by taking an initial uncompressed or distortion-free image as reference. Usually the larger the value is, the less distortion the image is and the more similar the two images are. It is based on three comparison measurements between images x and y: luminance l, contrast c and structure s [56].

$$SSIM(x, y) = l(x, y)c(x, y)s(x, y). \tag{23}$$

Table 4 lists the results of evaluation metric by RMS contrast, with respect to the eighteen images used in analysis of visual effect. Six methods including MSRCR, RCP, UDCP, GAN, RAHIM and the proposed method in the study are compared. Table 5 presents the results by UCIQE metric. Table 6 presents the results by PSNR metric and

TABLE 4. Evaluation of processed images by metric RMS contrast.

Image	Original	MSRCR	RCP	UDCP	GAN	RAHIM	Proposed
No.1	2.3521	7.4528	6.5999	6.5849	2.7318	**18.2059**	12.3210
No.2	2.1826	3.3895	3.0383	3.1318	6.7154	**11.2286**	4.8333
No.3	1.9478	3.9599	2.6177	2.9624	4.5384	**16.5310**	6.5189
No.4	3.8181	5.5341	6.0301	5.6879	5.9773	**16.5779**	14.1931
No.5	4.4942	5.1946	5.2615	4.4885	6.4189	**13.7111**	8.0306
No.6	8.7660	7.1920	10.1545	9.3443	14.7745	**30.2725**	18.6592
No.7	2.5158	4.5260	4.7543	3.7081	5.5841	**21.4789**	8.5152
No.8	2.6252	4.2842	3.5708	3.5495	3.6328	**12.9927**	5.6520
No.9	2.1521	5.1250	5.5719	5.0576	2.7970	**15.3498**	9.3742
No.10	4.1857	10.6887	8.0808	9.4375	4.8070	**19.3310**	13.8022
No.11	3.5719	6.5206	5.6562	6.5936	6.9564	**17.1783**	13.2289
No.12	2.7518	4.4605	3.9306	4.2798	2.6715	**10.9863**	7.7673
No.13	11.4038	12.2922	11.8579	13.631	16.5827	**25.8412**	24.2269
No.14	4.6284	8.1769	7.8495	8.4089	6.3399	**19.5036**	16.5877
No.15	3.9510	6.6831	7.8847	7.1418	5.2474	**16.9571**	14.7542
No.16	2.6735	4.8647	4.6965	4.8029	2.3417	**16.9751**	9.2889
No.17	3.5140	6.4768	6.1803	6.2725	4.2346	**18.2889**	15.5024
No.18	3.8134	6.3255	6.8544	6.6750	4.9547	**21.3856**	14.7697

TABLE 5. Evaluation of processed images by metric UCIQE.

Image	Original	MSRCR	RCP	UDCP	GAN	RAHIM	Proposed
No.1	0.2492	0.2771	0.3233	0.3255	0.1847	**0.4666**	0.3407
No.2	0.4416	0.4930	0.5181	0.5225	0.4215	0.4882	**0.5609**
No.3	0.3700	0.4802	0.4508	0.4945	0.3992	0.4876	**0.4904**
No.4	0.3475	0.3056	0.4361	0.3793	0.3770	0.4316	**0.5791**
No.5	0.3666	0.3533	0.4706	0.4686	0.4007	0.4460	**0.5450**
No.6	0.3392	0.2319	0.3579	0.3509	0.2773	0.4634	**0.4660**
No.7	0.2407	0.3410	0.3983	0.3492	0.2886	0.4377	**0.5197**
No.8	0.2632	0.3295	0.3860	0.4091	0.2122	0.4169	**0.5096**
No.9	0.1942	0.4234	0.4376	0.4115	0.2458	0.4259	**0.5278**
No.10	0.3287	0.3393	0.3445	0.3905	0.2703	0.4237	**0.5237**
No.11	0.2514	0.3750	0.3496	0.3892	0.2242	0.4749	**0.5061**
No.12	0.2827	0.4192	0.4129	0.4598	0.2100	0.4497	**0.5393**
No.13	0.3969	0.3335	0.3783	0.4034	0.3987	0.4684	**0.5003**
No.14	0.2666	0.3430	0.3523	0.3753	0.2255	0.4828	**0.5293**
No.15	0.3316	0.3920	0.4589	0.4197	0.2378	**0.4694**	0.2033
No.16	0.2701	0.4218	0.4159	0.4509	0.1536	0.4337	**0.5092**
No.17	0.2692	0.3050	0.3456	0.3194	0.3174	0.4891	**0.4904**
No.18	0.2634	0.3516	0.4223	0.3623	0.3211	0.4752	**0.4798**

Table 7 presents the results by SSIM metric. From the comparison results, it can be seen that among four methods to be compared, i.e., MSRCR, RCP, UDCP, and GAN, MSRCR gains over the others generally. In fact, MSRCR is preferred for many researchers to conduct image enhancement. Nevertheless, it should be noted that in general the proposed algorithm in the study presents a better performance than MSRCR, so than RCP, UDCP, and GAN, no matter which metric is employed to evaluate the image enhancement algorithms. Minor exceptions include: in Table 4, RMS value of image No. 2 processed by GAN is larger than the proposed algorithm. In Table 5, the UCIQE value of image No.3 processed by UDCP is slightly greater than the proposed algorithm. In table 6, the PSNR values of three images (No.10, 11, 13) by MSRCR are slightly smaller than the proposed algorithm, while the PSNR values of three images (No.4, 6, 15) by MSRCR are smaller than the proposed algorithm to some extent. In fact, from the view point of visual effect

TABLE 6. Evaluation of processed images by metric PSNR.

Image	MSRCR	RCP	UDCP	GAN	RAHIM	Proposed
No.1	10.5662	15.5663	15.2659	17.1786	12.1638	**9.4486**
No.2	21.1825	18.8164	16.4701	18.2037	17.7636	**14.5688**
No.3	11.1632	15.4334	12.7277	14.2817	13.1827	**10.5834**
No.4	**7.6367**	12.5247	14.2971	12.8451	10.2523	9.4418
No.5	9.9329	14.0923	16.7474	12.7271	9.92166	**9.1190**
No.6	**10.9984**	18.3644	23.4144	17.4907	13.8755	13.3042
No.7	16.7459	18.2300	15.9869	15.9770	**12.9940**	14.6083
No.8	16.8213	13.5497	14.4618	12.5364	13.1437	**10.8987**
No.9	16.3171	15.6543	16.3298	15.7753	13.5196	**12.5515**
No.10	**9.7089**	11.4911	11.4911	13.6427	10.6525	9.8158
No.11	12.7930	15.9783	17.6116	17.6946	**12.0833**	13.0051
No.12	14.8688	16.4301	15.1201	15.5810	13.8199	**13.0058**
No.13	**12.5756**	22.3345	24.0188	16.1566	12.7606	13.8585
No.14	15.0904	19.7551	20.5750	16.3132	13.5387	**12.9493**
No.15	**9.9744**	13.5865	15.3168	16.7522	11.6600	12.4385
No.16	13.3070	14.7867	14.8898	13.9261	12.9126	**11.6232**
No.17	18.9005	16.0915	14.1521	32.9200	13.8288	**13.0396**
No.18	22.3597	20.3330	17.5441	32.3601	14.2175	**14.9593**

TABLE 7. Evaluation of processed images by metric SSIM.

Image	MSRCR	RCP	UDCP	GAN	RAHIM	Proposed
No.1	0.6019	0.6664	0.6670	0.8365	**0.1918**	0.4687
No.2	0.6665	0.7440	0.8171	0.6363	**0.3599**	0.5650
No.3	0.6807	0.7479	0.7556	0.7081	**0.3082**	0.4429
No.4	0.5785	0.7007	0.7550	0.6460	**0.2237**	0.5158
No.5	0.6074	0.8217	0.9092	0.6405	**0.2652**	0.5152
No.6	0.5893	0.4524	0.9697	0.8151	**0.2342**	0.4968
No.7	0.8558	0.8304	0.8463	0.8637	**0.2505**	0.5354
No.8	0.8777	0.8014	0.8258	0.8508	**0.4228**	0.6090
No.9	0.7483	0.6895	0.7377	0.8876	**0.2559**	0.4281
No.10	0.6432	0.6659	0.6659	0.6802	**0.1869**	0.3722
No.11	0.7922	0.8565	0.8337	0.8933	**0.3218**	0.4894
No.12	0.7893	0.8287	0.7814	0.8787	**0.3541**	0.5302
No.13	0.7891	0.9340	0.9651	0.7855	**0.3520**	0.6203
No.14	0.8152	0.8775	0.8555	0.8719	**0.2967**	0.4786
No.15	0.6703	0.7094	0.7790	0.8344	**0.3167**	0.5094
No.16	0.7077	0.7609	0.7383	0.8366	**0.2878**	0.4774
No.17	0.9123	0.8841	0.8559	0.8748	**0.2858**	0.5486
No.18	0.9244	0.8935	0.8782	0.8426	**0.2578**	0.6027

with respect to these six images, the proposed algorithm outperforms MSRCR. Moreover, it should be noted that PSNR ignores the visual characteristics of human eyes. As a result, the evaluation results are sometimes inconsistent with human subjective perception. Different from the absolute-error based PSNR, SSIM is a perception-based method for predicting the perceived quality of images. By comparing the visual effects of the six images (No. 4, 6, 10, 11, 13, 15) as shown in Fig.6, the proposed algorithm in the study outperforms MSRCR. This can also be confirmed by SSIM metric listed in Table 7. Obviously, the SSIM values in the last column are the smallest among all values with MSRCR, RCP, UDCP, and GAN.

In RAHIM algorithm, Rayleigh distribution based overlapping histogram processing is performed to enhance underwater images, mainly in the aspects of contrast and color. As a result, the contrast of an image can be significantly improved. This is can be confirmed by the results in Table 4 and Table 7 , from which one can recognize that for RAHIM the metrics RMS and SSIM are the best. However, it should be noted that due to the aforementioned instability of RAHIM, some values w.r.t RAHIM are non-meaningful any more although they seem to be the best. For example, distortion happens to the image No.2, over-enhancement happens to the image No.1 and No.18 by using RAHIM (as can be seen from Fig.6), however the corresponding RMS and SSIM values obtained by RAHIM algorithm are seemingly significantly better than the other algorithms. In terms of a comprehensive metric UCIQE, except for the first image (No.1), the proposed algorithm is better than RAHIM. Moreover, for the PSNR metric listed in Table 6 , the proposed method outperforms RAHIM in general.

V. CONCLUSION

This paper proposes a fusion algorithm for underwater image restoration and enhancement, in which color balance, contrast optimization and histogram stretching based on red channel are combined. By comparing the histogram distribution characteristics of underwater images and foggy images in air, a novel color correction algorithm is proposed to eliminate the color deviation of underwater images. Then, an optimized contrast algorithm is used for image dehazing. According to the characteristics of underwater light attenuation, a modified histogram algorithm based on red channel is proposed to improve the contrast and clarity of underwater images after dehazing. Through the proposed fusion algorithm, underwater images are enhanced by eliminating color deviation, ambiguity and improving contrast. Experiments demonstrate the effectiveness and versatility of the proposed method. Moreover, the proposed algorithm is compared with some traditional algorithms including MSRCR, RCP, UDCP, a modern algorithm GAN and RAHIM. Comparison results proves the advantages of the proposed algorithm over the other algorithms, both in terms of capability and robustness. Besides the visual effect evaluation, objective metrics including RMS, UCIQE, PSNR and SSIM are also used to evaluate the effectiveness and merits of the proposed fusion algorithm.

It should be noted although the algorithm proposed in this study shows better enhancement effect than other algorithms, it requires more processing time. The real-time performance cannot be guaranteed especially when dealing with a large number of images. Comparatively, it is more suitable at the preprocessing stage.

In future work, efforts will be devoted to the further treatment of the removal of noise in images and the improvement of the real-time performance of the proposed algorithm. Research on the real-time underwater object detection or tracking based on the recovered images will also be carried out.

REFERENCES

[1] M. Boudhane and B. Nsiri, "Underwater image processing method for fish localization and detection in submarine environment," *J. Vis. Commun. Image Represent.*, vol. 39, pp. 226–238, Aug. 2016.
[2] J. Ahn, S. Yasukawa, T. Sonoda, T. Ura, and K. Ishii, "Enhancement of deep-sea floor images obtained by an underwater vehicle and its evaluation by crab recognition," *J. Mar. Sci. Technol.*, vol. 22, no. 4, pp. 758–770, Dec. 2017.
[3] H. Singh, J. Adams, D. Mindell, and B. Foley, "Imaging underwater for archaeology," *J. Field Archaeol.*, vol. 27, no. 3, pp. 319–328, Jan. 2000.
[4] J.-I. Watanabe, Y. Shao, and N. Miura, "Underwater and airborne monitoring of marine ecosystems and debris," *J. Appl. Remote Sens.*, vol. 13, no. 4, Oct. 2019, Art. no. 044509.

[5] L. Gu, Q. Song, H. Yin, and J. Jia, "An overview of the underwater search and salvage process based on ROV," *Sci. Sinica Inf.*, vol. 48, no. 9, pp. 1137–1151, Sep. 2018.

[6] S. Hong, S. Fang-Jian, C. Bo, and Q. Wei, "An underwater ship fault detection method based on sonar image processing," *J. Phys., Conf. Ser.*, vol. 679, Oct. 2016, Art. no. 012036.

[7] O. G. Powar, "A review: Underwater image enhancement using dark channel prior with gamma correction," *Int. J. Res. Appl. Sci. Eng. Technol.*, vol. 5, no. 3, pp. 421–426, Mar. 2017.

[8] M. Silver, "Marine snow: A brief historical sketch," *Limnol. Oceanogr. Bull.*, vol. 24, no. 1, pp. 5–10, Feb. 2015.

[9] M. Koziarski and B. Cyganek, "Marine snow removal using a fully convolutional 3D neural network combined with an adaptive median filter," in *Proc. ICPR*, Beijing, China, 2018, pp. 16–25.

[10] B. Cyganek and K. Gongola, "Real-time marine snow noise removal from underwater video sequences," *J. Electron. Imag.*, vol. 27, no. 4, Jul. 2018. Art. no. 043002.

[11] D.-M. He and G. G. L. Seet, "Divergent-beam lidar imaging in turbid water," *Opt. Lasers Eng.*, vol. 41, no. 1, pp. 217–231, Jan. 2004.

[12] B. Ouyang, F. Dalgleish, A. Vuorenkoski, W. Britton, B. Ramos, and B. Metzger, "Visualization and image enhancement for multistatic underwater laser line scan system using image-based rendering," *IEEE J. Ocean. Eng.*, vol. 38, no. 3, pp. 566–580, Jul. 2013.

[13] R. Schettini and S. Corchs, "Underwater image processing: State of the art of restoration and image enhancement methods," *EURASIP J. Adv. Signal Process.*, vol. 2010, Dec. 2010, Art. no. 746052.

[14] K. Iqbal, R. A. Salam, A. Osman, and A. Z. Talib, "Underwater image enhancement using an integrated colour model," *IAENG Int. J. Comput. Sci.*, vol. 34, no. 2, pp. 239–244, 2007.

[15] B. Henke, M. Vahl, and Z. Zhou, "Removing color cast of underwater images through non-constant color constancy hypothesis," in *Proc. 8th Int. Symp. Image Signal Process. Anal. (ISPA)*, Trieste, Italy, Sep. 2013, pp. 20–24.

[16] G. Guraksin, O. Deperlioglu, and U. Kose, "A novel underwater image enhancement approach with wavelet transform supported by differential evolution algorithm," in *Nature Inspired Optimization Techniques for Image Processing Applications*. Cham, Switzerland: Springer, 2019, pp. 255–278.

[17] C. Tang, U. F. von Lukas, M. Vahl, S. Wang, Y. Wang, and M. Tan, "Efficient underwater image and video enhancement based on Retinex," *Signal, Image Video Process.*, vol. 13, no. 5, pp. 1011–1018, Jul. 2019.

[18] A. S. A. Ghani and N. A. M. Isa, "Underwater image quality enhancement through Rayleigh-stretching and averaging image planes," *Int. J. Nav. Archit. Ocean Eng.*, vol. 6, no. 4, pp. 840–866, Dec. 2014.

[19] A. S. A. Ghani and N. A. M. Isa, "Underwater image quality enhancement through integrated color model with Rayleigh distribution," *Appl. Soft Comput.*, vol. 27, pp. 219–230, Feb. 2015.

[20] A. S. A. Ghani and N. A. M. Isa, "Enhancement of low quality underwater image through integrated global and local contrast correction," *Appl. Soft Comput.*, vol. 37, pp. 332–344, Dec. 2015.

[21] M. N. M. J. Noordin, N. A. M. Isa, and W. H. Lim, "Saturation avoidance color correction for digital color images," *Multimedia Tools Appl.*, vol. 76, no. 7, pp. 10279–10312, Apr. 2017.

[22] A. S. A. Ghani and N. A. M. Isa, "Automatic system for improving underwater image contrast and color through recursive adaptive histogram modification," *Comput. Electron. Agricult.*, vol. 141, pp. 181–195, Sep. 2017.

[23] J. Perez, A. C. Attanasio, N. Nechyporenko, and P. J. Sanz, "A deep learning approach for underwater image enhancement," in *Proc. IWINAC*, Corunna, Spain, 2017, pp. 183–192.

[24] Y. Wang, J. Zhang, Y. Cao, and Z. Wang, "A deep CNN method for underwater image enhancement," in *Proc. IEEE Int. Conf. Image Process. (ICIP)*, Beijing, China, Sep. 2017, pp. 1382–1386.

[25] S. Anwar, C. Li, and F. Porikli, "Deep underwater image enhancement," 2018, *arXiv:1807.03528*. [Online]. Available: https://arxiv.org/abs/1807.03528

[26] P. Liu, G. Wang, H. Qi, C. Zhang, H. Zheng, and Z. Yu, "Underwater image enhancement with a deep residual framework," *IEEE Access*, vol. 7, pp. 94614–94629, 2019.

[27] C. Fabbri, M. J. Islam, and J. Sattar, "Enhancing underwater imagery using generative adversarial networks," in *Proc. IEEE Int. Conf. Robot. Automat. (ICRA)*, Brisbane, QLD, Australia, May 2018, pp. 7159–7165.

[28] Y. Guo, H. Li, and P. Zhuang, "Underwater image enhancement using a multiscale dense generative adversarial network," *IEEE J. Ocean. Eng.*, vol. 45, no. 3, pp. 862–870, Jul. 2020.

[29] A. S. A. Ghani, "Image contrast enhancement using an integration of recursive-overlapped contrast limited adaptive histogram specification and dual-image wavelet fusion for the high visibility of deep underwater image," *Ocean Eng.*, vol. 162, pp. 224–238, Aug. 2018.

[30] C. Ancuti, C. O. Ancuti, T. Haber, and P. Bekaert, "Enhancing underwater images and videos by fusion," in *Proc. IEEE Conf. Comput. Vis. Pattern Recognit.*, Providence, RI, USA, Jun. 2012, pp. 81–88.

[31] X. Qiao, J. Bao, H. Zhang, L. Zeng, and D. Li, "Underwater image quality enhancement of sea cucumbers based on improved histogram equalization and wavelet transform," *Inf. Process. Agricult.*, vol. 4, no. 3, pp. 206–213, Sep. 2017.

[32] E. Trucco and A. T. Olmos-Antillon, "Self-tuning underwater image restoration," *IEEE J. Ocean. Eng.*, vol. 31, no. 2, pp. 511–519, Apr. 2006.

[33] J. S. Jaffe, "Computer modeling and the design of optimal underwater imaging systems," *IEEE J. Ocean. Eng.*, vol. 15, no. 2, pp. 101–111, Apr. 1990.

[34] N. Wang, L. Qi, J. Dong, H. Fan, X. Chen, and H. Yu, "Two-stage underwater image restoration based on a physical model," in *Proc. 8th Int. Conf. Graph. Image Process. (ICGIP)*, Tokyo, Japan, Feb. 2017, Art. no. 102250R.

[35] W. Barros, E. R. Nascimento, W. V. Barbosa, and M. F. M. Campos, "Single-shot underwater image restoration: A visual quality-aware method based on light propagation model," *J. Vis. Commun. Image Represent.*, vol. 55, pp. 363–373, Aug. 2018.

[36] Z. H. Shi, Y. N. Feng, M. H. Zhao, E. H. Zhang, and L. He, "Normalised gamma transformation-based contrast-limited adaptive histogram equalisation with colour correction for sand–dust image enhancement," *IET Image Process.*, vol. 14, no. 4, pp. 747–756, Nov. 2019.

[37] K. He, J. Sun, and X. Tang, "Single image haze removal using dark channel prior," *IEEE Trans. Pattern Anal. Mach. Intell.*, vol. 33, no. 12, pp. 2341–2353, Dec. 2011.

[38] N. Carlevaris-Bianco, A. Mohan, and R. M. Eustice, "Initial results in underwater single image dehazing," in *Proc. OCEANS MTS/IEEE SEATTLE*, Seattle, WA, USA, Sep. 2010, pp. 1–8.

[39] A. Galdran, D. Pardo, A. Picón, and A. Alvarez-Gila, "Automatic red-channel underwater image restoration," *J. Vis. Commun. Image Represent.*, vol. 26, pp. 132–145, Jan. 2015.

[40] L. Wang, W. Xie, and J. Pei, "Patch-based dark channel prior dehazing for RS multi-spectral image," *Chin. J. Electron.*, vol. 24, no. 3, pp. 573–578, Jul. 2015.

[41] I. Kansal and S. S. Kasana, "Minimum preserving subsampling-based fast image de-fogging," *J. Mod. Opt.*, vol. 65, no. 18, pp. 2103–2123, Oct. 2018.

[42] H. Yu, X. Li, Q. Lou, C. Lei, and Z. Liu, "Underwater image enhancement based on DCP and depth transmission map," *Multimedia Tools Appl.*, vol. 79, nos. 27–28, pp. 20373–20390, Jul. 2020.

[43] R. Liu, X. Fan, M. Zhu, M. Hou, and Z. Luo, "Real-world underwater enhancement: Challenges, benchmarks, and solutions under natural light," *IEEE Trans. Circuits Syst. Video Technol.*, vol. 30, no. 12, pp. 4861–4875, Dec. 2020, doi: 10.1109/TCSVT.2019.2963772.

[44] X. Zhang and L. Hu, "Effects of temperature and salinity on light scattering by water," *Proc. SPIE*, vol. 7678, no. 1, pp. 247–252, 2010.

[45] K. J. Voss, "Simple empirical model of the oceanic point spread function," *Appl. Opt.*, vol. 30, no. 18, pp. 2647–2651, 1991.

[46] J. McLean and K. Voss, "Point spread function in ocean water: Comparison between theory and experiment," *Appl. Opt.*, vol. 30, no. 15, pp. 2027–2030, 1990.

[47] J.-H. Kim, W.-D. Jang, J.-Y. Sim, and C.-S. Kim, "Optimized contrast enhancement for real-time image and video dehazing," *J. Vis. Commun. Image Represent.*, vol. 24, no. 3, pp. 410–426, 2013.

[48] W. Q. Wen, "Underwater image enhancement based on color compensation," M.S. thesis, Dept. Inf. Eng., Nanchang Hangkong Univ., Nanchang, China, 2018.

[49] M. J. Islam, Y. Xia, and J. Sattar, "Fast underwater image enhancement for improved visual perception," *IEEE Robot. Autom. Lett.*, vol. 5, no. 2, pp. 3227–3234, Apr. 2020.

[50] L. Han, Y. Tian, and Q. Qi, "Research on edge detection algorithm based on improved sobel operator," in *Proc. MATEC Web Conf.*, vol. 309, Mar. 2020, Art. no. 03031.

[51] E. Peli, "Contrast in complex images," *J. Opt. Soc. Amer. A, Opt. Image Sci.*, vol. 7, no. 10, pp. 2032–2040, 1990.

[52] W. F. Schreiber, *Fundamentals of Electronic Imaging Systems: Some Aspects of Image Processing*. New York, NY, USA: Springer, 1993, pp. 60–70.

[53] A. A. Michelson, *Studies in Optics*. New York, NY, USA: Dover, 1995.
[54] M. Yang and A. Sowmya, "An underwater color image quality evaluation metric," *IEEE Trans. Image Process.*, vol. 24, no. 12, pp. 6062–6071, Dec. 2015.
[55] A. Hore and D. Ziou, "Image quality metrics: PSNR vs. SSIM," in *Proc. 20th Int. Conf. Pattern Recognit.*, Istanbul, Turkey, Aug. 2010, pp. 2366–2369.
[56] Z. Wang, E. P. Simoncelli, and A. C. Bovik, "Multiscale structural similarity for image quality assessment," in *Proc. 37th Asilomar Conf. Signals, Syst. Comput.*, Pacific Grove, CA, USA, Nov. 2003, pp. 1398–1402.

WEILIN LUO (Member, IEEE) received the B.S. degree in mechanical manufacturing process and equipment from the Jiaozuo Institute of Technology, China, in 1995, the M.S. degree in solid mechanics from Fuzhou University, China, in 2003, and the Ph.D. degree in design and manufacture of naval architecture and ocean structure from Shanghai Jiao Tong University (SJTU), China, in 2009. From July 2012 to July 2013, he worked as a Postdoctoral Fellow with the University of Lisbon, Portugal. From March 2016 to March 2017, he visited the University of California at Berkeley (UC Berkeley), as a Research Scholar. Since 2017, he has been a Professor with the College of Mechanical Engineering and Automation, Fuzhou University, China. His research interests include ship maneuvering and control, underwater robotics, and artificial intelligent techniques.

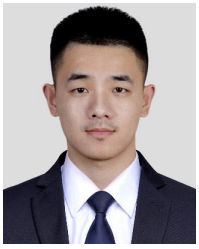

SHUNQIANG DUAN received the B.S. degree in mechanical manufacturing process and equipment from Wanxi Institute, China, in 2017. He is currently pursuing the master's degree in mechanical design and theory with Fuzhou University. His research interests include image processing and underwater techniques.

JIWEN ZHENG received the B.S. degree in mechanical manufacturing process and equipment from the Shandong Institute of Technology, China, in 2017, and the M.S. degree in mechanical engineering from Fuzhou University, China, in 2020. His research interest includes image processing.